AUTHORS:
Akwasi Boadu[1,2] (ID)
Rajshekhar Karpoormath[1] (ID)
Manimbulu Nlooto[1,3] (ID)

AFFILIATIONS:
[1]Synthetic and Medicinal Chemistry Research Group, Department of Pharmaceutical Chemistry, Discipline of Pharmaceutical Sciences, School of Health Sciences, University of KwaZulu-Natal, Durban, South Africa
[2]Physical Sciences Department, Wesbury College of Science, Port Shepstone, South Africa
[3]Department of Pharmacy, School of Health Care Sciences, University of Limpopo, Polokwane, South Africa

CORRESPONDENCE TO:
Akwasi Boadu

EMAIL:
concordf14@gmail.com

3 GOOD HEALTH AND WELL-BEING

Pharmaco-phytochemistry of esters isolated from leaf extracts of *Spondias mombin* as potential antiviral agents

The present work reports on the isolation and characterisation of two novel antiviral ester compounds from dichloromethane leaf extracts of *Spondias mombin* (*SM*). The characterisation and structural elucidation were established from spectroscopic evidence of nuclear magnetic resonance, Fourier transform infrared and mass spectroscopy. The compounds identified were 6-methylheptyl pentadecanoate and 6-methylheptyl-15-(1,2,3,4,4a,8a-hexahydronaphthalen-1-yl)pentadecanoate. The novel isolated ester compounds were reported to have anti-rhino virus activity *in silico* against a known biological target (HsNMT1) that plays a key role in developing therapeutics against the common cold. Molecular docking analysis revealed the binding affinity across all targets within the range of −4.6 to −8.2 kcal/mol, whilst molecular dynamic simulation showed that systems attained good stability due to the maintenance of mean root-mean-square deviation values within the acceptable range of 1.5−2.5 Å. It can be concluded that the novel compounds are potential inhibitory candidates against rhinovirus protein target HsNMT1. However, in vitro and in vivo experiments are further required to validate the possible inhibitory candidates against rhinovirus disease (common cold).

Significance:
The significance of this study contributes to the scientific rationale for using *SM* leaf extracts to treat viral diseases. Two novel compounds, 6-methylheptyl pentadecanoate and 6-methylheptyl-15-(1,2,3,4,4a,8a-hexahydronaphthalen-1-yl)pentadecanoate, were predicted through computer-aided techniques to possess anti-rhinovirus properties.

Introduction

Novel phytochemical compounds have diverse phytochemical and pharmacological properties. These phytochemicals are abundant in natural products[1], with some used as new drugs, leading to drug discovery[2]. The combination of ethnomedicinal uses, phytochemistry and pharmacological properties of crude, fractionated and/or isolated, pure compounds against numerous biological targets has led to the discovery of numerous drugs for treating infectious diseases.[3-5] Natural products, such as *Spondias mombin* (Anacardiaceae; *SM*) leaf extracts, have been used to treat several infectious diseases.[6] The pharmacological activities of leaf extracts of *S. mombin* have been attributed to some bioactive compounds isolated from the medicinal plant. Some of these isolated compounds from leaf extracts of *S. mombin* include esters such as 3β-olean-12-en-3-yl (9Z)-hexadec-9-enoate[7], chlorogenic acid butyl ester[8] and caffeoyl ester[9,10]. The leaves are reported to be part of the medicinal plant, and are mostly used for treating viral respiratory infections such as rhinovirus in traditional African healing systems.[11]

Human rhinoviruses affect the upper and lower respiratory tract and cause common colds associated with pneumonia, wheezing and asthma.[12]

Isolated compounds from natural products are identified by several chromatographic and spectroscopic methods, such as thin layer chromatography (TLC), column chromatography (CC), Fourier transform infrared (FTIR) spectroscopy, gas chromatography and mass spectroscopy (GC–MS) and nuclear magnetic resonance (NMR), among others. These methods for the separation, identification and structural determination of phytochemicals are becoming increasingly powerful.[13] TLC might be the simplest of all chromatographic methods, but it provides critical information for identifying compounds separated by other methods during the phytochemistry analysis of natural products.[14]

FTIR is known to identify only the types of functional groups in a compound, most commonly CH_2, CH_3, $=CH$, $\equiv CH$, O–H, C=O, C–O, C=C, C≡C, C–O–C and C–C–O.[15] FTIR and NMR analysis, coupled with mass spectroscopy (MS), are helpful tools in the structural elucidation of an isolated compound.

In order to assess the therapeutic potential of the selected compounds via *in silico* methods, it was necessary to identify a peculiar biological target. The prediction of the biological activities of the compounds was determined by utilising the PASSonline software.[16] This software is used for the prediction of different physiological activities for multiple compounds, both natural and synthetic, based on their chemical formula. Additionally, PASSonline predicts pharmacological effects, mechanisms of action, adverse effects, interaction with metabolic enzymes and transporters, and influence on gene expression. It uses the 2D molecular fragments known as multilevel neighbours of atom descriptors, which postulates that a compound's molecular structure may determine whether it is biological.[17] With this software, the evaluated activity of a compound is estimated as probable activity (Pa) and probable inactivity (Pi).[18]

We aimed to isolate, identify, characterise and predict the antiviral properties of novel esters using computer-aided drug design methods on novel inhibitors of human rhinovirus protease through molecular docking and molecular dynamic simulation. The results reveal, for the first time, two ester compounds from *S. mombin* leaf extracts that possess antiviral properties in an *in silico* molecular target prediction.

Methods

Material processing and extraction

Fresh leaves of *S. mombin* Linn were collected from Cape Coast, Ghana, and authenticated. Leaves dried at room temperature were pulverised by using a hammer mill. The leaf powder of mass 100 g was initially defatted with 1 L of hexane and then extracted with 2 L DCM by cold maceration for 72 h until the solvent was clear. The extracts were filtered with filter paper and concentrated using a rotary evaporator under reduced pressure at 40 °C. The concentrate was completely dried with a weight of 5.19 g (5.17%) and denoted as *SM*-DCM.

General analytical information

^{1}H and ^{13}C NMR spectra were recorded on a Bruker AV 400 MHz instrument at 400 MHz (^{1}H NMR) and 100 MHz (^{13}C NMR). All ^{1}H NMR spectra were measured in parts per million (ppm) downfield or relative to the residual proton signals of d1-chloroform (CDCl$_3$, 7.26 ppm). All ^{13}C NMR spectra were reported in ppm relative to the residual carbon signals of CDCl$_3$ (77.16 ppm). Coupling constants (J) are reported in Hertz (Hz). Multiplicity is indicated as follows: s (singlet), d (doublet), t (triplet), q (quartet), p (pentet) and m (multiplet).[15] Thin layer chromatography (TLC) was performed on precoated Merck Silica gel 60 F254 plates using different polarities of hexane-ethyl acetate solvent systems, and compounds were visualised with UV light at 254 nm.[19] The retention factor (R$_f$) values of the different spots that were observed were calculated.[20]

The R$_f$ values were calculated using Equation 1:

$$R_f = \frac{Distance\ traveled\ by\ the\ solute}{Distance\ traveled\ by\ the\ solvent} \qquad \text{Equation 1}$$

FTIR spectroscopy was performed using a PerkinElmer Spectrum 100 spectrophotometer at room temperature, whilst the MS of isolates was determined using a CombiFlash Purlon Mass Spectrometer (2000 Da Polarity Auto Switching).

Preliminary phytochemical screening of SM-DCM extract

Preliminary phytochemical screening was performed as a qualitative process to investigate the presence of different classes of phytochemicals according to standard procedures as reported by other authors.[21,22] Briefly, crude DCM leaf extract of *S. mombin* was used for the qualitative analysis to determine the presence of alkaloids, steroid flavonoids, saponins, terpenoid tannins, anthraquinone derivatives and cardiac glycosides.

Column fractionation of SM-DCM mixture

The *S. mombin* DCM extract was loaded onto a glass column packed with silica gel. It was then eluted with mixtures of ethyl acetate and hexane of increasing gradient polarity, starting with 100% hexane to 100% ethyl acetate. One hundred and seventy-one fractions were collected in 50 mL aliquots. Based on their TLC analysis, aliquots 55–100 with a similar R$_f$ value (retention factor), were bulked together (denoted C) for further separation of the two compounds. It was further separated using column chromatography with silica gel using a solvent mixture of gradient, ethyl acetate and hexane. Seventy fractions were collected in 10 mL aliquots, and based on the TLC, aliquots 1–23 were bulked into CS1 and 24 to 70 into CS2.

Characterisation of isolated compounds

Chemical shifts are reported for DSS-trimethyl singlet resonance at 0.0000 ppm and multiplicity.

Characterisation of 6-methylheptyl pentadecanoate (CS1)

A dark green solid, 6-methylheptyl pentadecanoate (CS1): FTIR (KBr) νmax cm^{-1}: 2927 (CH$_2$), 1748(C=O), 1465 (CH bending), 1220 (C–O), 725 (CH). ^{1}H NMR (CDCl$_3$, 400 MHz) δ^1**H** (ppm): 3.96 (2 H, q, J = 2.56 Hz, H-8), 2.30 (2 H, q, J = 4.72 Hz, H-10), 1.64 (1 H, m, H-11), 1.55 (1 H, q, J = 5.96 Hz, H-2), 1.30 (30 H, m, H4–7, H-11–21), 0.90 (12 H, m, H1&3, H23&22). ^{13}C NMR (CDCl$_3$, 400 MHz) δ^{13}C (ppm):

173.57 (C-11), 79 (C-10), 68 (C-9), 40 (C-8), 36 (C-7), 35 (C-6), 32 (C-5), 30 (C-4), 22–25 (C-3), 14.03–14.11 (C-2), 10.97 (C-1).

Characterisation of 6-methylheptyl 15-(1,2,3,4,4a,8a-hexahydronaphthalen-1-yl) pentadecanoate (CS2)

A dark green solid, 6-methylheptyl 15-(1,2,3,4,4a,8a-hexahydronaphthalen-1-yl)pentadecanoate (CS2): FTIR (KBr) νmax cm^{-1}: 2927 (CH$_2$), 1748 (C=O), 1465 (C–H bending), 1220 (C–O), 725 (C–H). ^{1}H NMR (CDCl$_3$, 400 MHz) δ^1**H** (ppm): 7.66 (1 H, J = 2.4 Hz, H-5), 7.12 (1 H, d, J = 8.8 Hz, H-6), 6.8 (1 H, J = 8.8 Hz, H-7), 4.16 (1 H, d, J = 3.32 Hz, H-10), 3.97 (1 H, J = 2.32 Hz, H-4), 3.96 (1 H, J = 3.42 Hz, H-8), 3.63 (1 H, d, J = 5.92 Hz), 3.30 (1 H, d, J = 5.8 Hz), 2.29 (1 H, d, J = 5.84 Hz, H-9), 1.53 (2 H, d, J = 3.52 Hz, H-18), 1.26 (25 H, m H-19, 20, 22, 25–28), 0.86 (10 H, m H-24).^{13}C NMR (CDCl$_3$, 400 MHz). δ^{13}C (ppm): 173.57 (C-9), 127.58 (C-33), 114.03 (C-30), 66.81 (C-8), 38.74 (C-18), 34.00 (C-17), 31.93 (C-16), 30.41 (C-15), 29.70 (C-14), 29.66 (C-13), 29.36 (C-12), 28.92 (C-11), 24.48 (C-7), 23.79 (C-6), 22.96 (C-5), 22.69 (C-4), 14.11 (C-3), 14.04 (C-2), 10.98 (C- 1).

Biological activity prediction via PASSonline

PASSonline software[16] is used to predict physiological activities, pharmacological effects, mechanisms of action, toxic and adverse effects, interaction with metabolic enzymes and transporters and influence on gene expression for multiple compounds, both natural and synthetic, based on their chemical formula.

The evaluated activity of a compound is estimated as Pa and Pi.[18] Compounds presenting Pa higher than Pi relative to a particular activity are considered feasible for that specific medical activity, and those with Pi higher than Pa are, therefore, eliminated. To this end, the selected compounds were assessed for their biological activities on PASSonline.

Molecular docking

The X-ray crystal structures of some selected rhinovirus antiviral targets (PDB ID: 5FX6, 5MU6, 4C2X and 1CQQ)[23] were retrieved from the Protein Data Bank[24]. These structures were co-crystallised with native inhibitors that defined their respective binding sites. The structures, 5FX6, 5MU6, 4C2X and 1CQQ, were then prepared by using UCSF Chimera version 1.13.1[25] to remove all non-standard residues, and Modeller 9.25 version[26] was employed to fix missing residues. The binding site residues were obtained by zoning the native inhibitors and selecting residues that lie within 5 Å for each target protein. Subsequently, the selected compounds were optimised using Avogadro 2.0 software and saved. Molecular docking was carried out for the three selected compounds against each of the rhinovirus target proteins using Prix software. The target that showed the best docking properties against all compounds was selected for molecular dynamics simulation.

Molecular dynamic simulation

Molecular dynamic (MD) simulations were performed using the AMBER18 GPU package for the best-docked ligand, CS1 and CS2, and IMP-1088 for the target (HsNMT1). The ligand and receptor were both defined and optimised using the AMBER force fields using the Antechamber and LEAP modules, respectively. Solvation and neutralisation were carried out on the receptor prior to its combination with the ligand. Partial minimisation of the receptor in the system was conducted for 2500 steps with a restraint potential of 500 kcal/mol Å2, followed by complete minimisation of 10 000. The system underwent heating at 300 K using a Langevin thermostat in a canonical ensemble (NVT). Equilibration of the system was carried out to ensure that AMBER rechecks the system, and it was at 300 K. MD simulation was run for 12 h at 100 ns, and results were obtained in the form of trajectories and analysed using statistics. The trajectories generated allow for the measurement of the binding energies of the association of the ligand with the receptor. The visualisation of the interactions was produced by Snapshots and Discovery Studio.

Binding free energy analysis via MM/GBSA method

The molecular mechanics/generalised-born surface area (MM/GBSA)[27,28] method was employed in estimating the binding free energy

for each of the inhibitor-bound systems. The binding free energy (ΔG_{bind}) was calculated from the following equations:

$$\Delta G_{bind} = G_{complex} - G_{receptor} - G_{ligand} \qquad \text{Equation 2}$$

$$\Delta G_{bind} = E_{gas} + \Delta G_{sol} - TS, \qquad \text{Equation 3}$$

where ΔG_{bind} is the summation of the gas phase and solvation energy terms less the entropy (TS) term.

$$E_{gas} = E_{int} + E_{vdw} + E_{lec} \qquad \text{Equation 4}$$

E_{gas} is the sum of the AMBER force field internal energy terms E_{int} (bond, angle and torsion), the covalent van der Waals (E_{vdw}) and the non-bonded electrostatic energy component (E_{lec}). The solvation energy is calculated from the following equation:

$$G_{sol} = G_{GB} + G_{non\text{-}polar} \qquad \text{Equation 5}$$

$$G_{non\_polar} = \gamma SASA + b \qquad \text{Equation 6}$$

where ΔG_{bind} is taken to be the sum of the gas phase and solvation energy terms less the entropy (TΔS) term and $G_{Complex}$ represents the energy of the receptor–ligand complex, whilst $G_{receptor}$ and G_{ligand} represent the energies of receptor and ligand, respectively. E_{gas} denotes gas-phase energy; E_{int} signifies internal energy; and E_{ele} and E_{vdw} indicate the electrostatic and van der Waals contributions, respectively. E_{gas} is the gas phase, elevated directly from the FF14SB force terms. G_{asol} denotes solvation-free energy and can be decomposed into polar and non-polar contribution states. The polar solvation contribution, G_{GB}, is determined by solving the GB equation, whereas G_{SA}, the non-polar solvation contribution, is estimated from the solvent-accessible surface area (SASA) determined using a water probe radius of 1.4 Å. T and S correspond to temperature and total solute entropy, respectively. γ is a constant.[29] Per-residue decomposition analyses were also carried out to estimate the individual energy contribution of residues in the substrate pocket towards the affinity and stabilisation of each target.

Results and discussion

Figures 1 and 3 show structures of isolated esters: 6-methylheptyl pentadecanoate and 6-methylheptyl 15-(1,2,3,4,4a,8a-hexahydronaph-thalen-1-yl)pentadecanoate from DCM leaf extracts of *S. mombin*. The FTIR, NMR and MS/MS spectra of the isolated compounds are provided in Supplementary figures 1–14.

Preliminary phytochemical screening and TLC test of compounds CS1 and CS2

Table 1 indicates a phytochemical test to examine the qualitative chemical constituents contained in leaf extracts of *S. mombin*. The phytochemical test revealed the presence of anthraquinone derivatives, steroids, tannins and cardiac glucosides. The results of the preliminary phytochemical screening are in line with reports by other authors.[30,31]

The percentage yield in this study was calculated using the weight of the extracted sample divided by the total sample used and found to be 11.14% (Table 2).

During the TLC test, the retention factor values obtained in this experiment (Table 3) did not give many clues as to the type of compounds in the

extract, but they did suggest the polarity of the compounds as reported by Talukdar et al.[14] The authors indicated that a high R_f value in a less polar solvent system possesses low polarity.[14]

Structural elucidation of 6-methylheptyl pentadecanoate (CS1)

The FTIR spectrum was used to identify the functional groups of the active components present in the extract based on the peak values in the region of IR radiation. When the extract was analysed by FTIR, the functional groups of the components were separated based on their peak ratio.

The peak values were recorded in Supplementary table 1 and Supplementary figure 1 for CS1, indicating the carbonyl group, which represents an ester with C=O stretch, was observed at 1748.0 cm^{-1} with very strong intensity (1750–1735 cm^{-1}).[36] This is in line with the reported carbonyl group of 1750 cm^{-1} by Wang et al.[36] At 1748.0 cm^{-1}, the peak assigned to C=O ester was confirmed by other researchers to be between 1734 and 1745 cm^{-1}.[37-39] An aliphatic ester O=C–O–C, with two bands, one stronger than the other, was also observed at 1220.0 cm^{-1} (1160–1210 cm^{-1}).[40,41] As noted, the two bands at 1220.0 cm^{-1}, with one stronger than the other, are attributed to the presence of an aliphatic ester C–O, although Jain et al.[42] assigned a C–O stretching at 1253.97 and 1054.89 cm^{-1}. Compound CS1 has bands at 2927.0 cm^{-1} that are due to the symmetric stretching of the SP^3 carbon (C–H stretch), this wavelength being reported by other authors at a figure between 2961 cm^{-1} and 2923 cm^{-1}.[39,42-44] Findings from this study revealed a band at 1465.0 cm^{-1}, indicating a C–H bending, although other investigators reported the C–H bending at 1470 cm^{-1}.[44]

Table 1: Preliminary phytochemical screening of *SM*-DCM extract

Class of phytochemicals	Tests performed	*Spondias mombin* leaf extracts *SM*-DCM
Alkaloids	Meyer	–
Anthraquinone derivatives	Bontrager test	+
Steroids	Liebermann-Burchard test	+
Terpenoids	Liebermann-Burchard test	–
Saponins	Frothing	–
Flavonoids	Sulfuric acid test	–
Tannins	Ferric chloride test	+
Cardiac glucosides	Keller Killian	+

Key: +, present; –, absent

Table 2: Physical appearance, weight of dry crude extract per solvent of extraction and percentage (%) yield from 60 g *SM* dry powder

Physical properties	*SM*-DCM leaf extract
Physical appearance	Yellowish green
Yield/weight of crude extract (g)	6.688 g
% Yield	11.14%

Table 3: Thin layer chromatography test of CS1 and CS2

Sample	Solvent phase	Distance travelled by solvent (cm)	Distance travelled by the solute (cm)	Experimental R_f values	R_f values literature	Colour of peaks
CS1	30% v/v hexane in ethyl acetate	2.8	2.0	0.714	0.71 (phenolics) [32-35]	dark
CS2	30% v/v hexane in ethyl acetate	2.8	1.3	0.464	–	dark

The NMR analysis of CS1, as referenced in Supplementary table 2, indicates that the proton shifts between carbons C1–C7 are aliphatic alkanes, with carbons C8, C10, C11 and C2 at 3.96 ppm (q, 2 H, J = 2.59 Hz, H-8)[45], 2.30 ppm (q, 2 H, J = 4.72 Hz, H-10)[6,46,47], 1.64 ppm (m, 1 H, H-11)[48], 1.55 (1 H, q, J = 5.96 Hz, H-2) with 0.9 ppm (m, 12 H, H1&3, H23&22)[48-51]. Carbon C8 is an alkyl (–CH_2) of the ester, with C10 showing a carbonyl ester group (O–CH_2); this is in line with the literature and reported to be an alkyl adjacent to a heteroatom (R–O–CH_2).[36,48,52] Proton on carbon C10, indicated two hydrogen quartets at 2.30 ppm, which is in line with reports by Buckingham[48], who also revealed a band at 2.30 ppm to be CH_3COR. The singlet hydrogen, occurring at 7.25 ppm (7.05–7.25 ppm), indicates a proposed functional group of $CR^3R^4R^3$.[48]

Supplementary table 4 indicates the analysis of the ^{13}C NMR spectrum for CS1, which revealed that the ^{13}C spectrum has approximately 16 carbon peaks (δ 10.97, 14.03–14.11, 22–25, 30, 32, 35, 36, 40, 68, 79 and 173.57 ppm), as expected given the top/bottom overlaps in the spectrum, with a strong carbonyl peak at 173.57 ppm assigned to carbon 9 (Figure 1).

The distortionless enhancement by polarisation transfer (DEPT-135), which shows all the resonances of protonated carbons, obviously distinguishes between the methyl (–CH_3) (14.11, 14.04 and 10.97 ppm), methine (CH) (38.74 ppm) and methylene[52] (–CH_2) (66.63, 34.01, 31.93, 30.41, 29.70, 29.37, 28.92, 24.49, 23.79, 22.99, 22.69 ppm)[52,53] of the ethyl chain (Supplementary figures 7 and 12). The peak, close to carbonyl at 66.63 ppm, was assigned to –CH_2– carbon 8, that of tertiary carbon two at 34.01 ppm, whilst primary carbons 1 and 3

also appeared at 14.11 ppm and 14.04 ppm, respectively. The rest of the methylene carbons 4–7 could be seen at 29.37– 31.93 ppm (Figure 4).

Electron ionisation mass spectroscopy (EIMS) of the isolated compound CS1 showed a mass ion peak at *m/z* 355 [M + H] (Supplementary figure 3), from which a molecular formula of $C_{23}H_{46}O_2$ was assigned. Typically, molecule CS1, at a retention time (Rt) of 0.714 min (Table 3), produces a precursor ion at *m/z* 355 [M + H], and the fragmentation of this molecule (Figure 2) generated product ions at *m/z* 298. These were derived from the loss of the isobutyl side chain (–57 Da) after a possible 1,3 methyl rearrangement of the isopropyl derivative of methylheptyl pentadecanoate to a more stable butyl pentadecanoate derivative (Figure 2). Product ions at *m/z* 284, due to the neutral loss of methyl (–14 Da), and at *m/z* 266 (loss of propyl molecule) were also observed. Based on these data, CS1 was identified as 6-methylheptyl pentadecanoate.

We, therefore, propose the structure and IUPAC name for compound CS1 based on the information obtained as 6-methylheptyl pentadecanoate.

The fragmentation pattern of 6-methylheptyl pentadecanoate was based on the analysis of mass spectroscopy in Supplementary figure 3. The fragmentation pattern is indicated below (Figure 2).

Structural elucidation of CS2

Similar to the FTIR analysis of Supplementary table 1 and Supplementary figure 2, compound 6-methylheptyl-15-(1,2,3,4,4a,8a-hexahydronaphthalen-1-yl)pentadecanoate (CS2) indicates that the isolated compound is an ester. Evidence of the presence of an ester
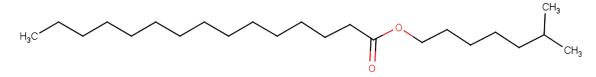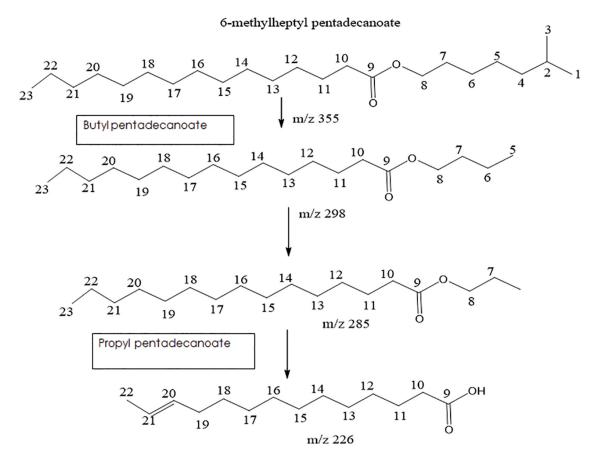

Figure 1: Proposed structure of CS1-Compound 1.

Figure 2: Fragmentation pattern of CS1 from mass spectroscopy.

showed peaks at 1748 cm⁻¹ and 1220 cm⁻¹, indicating the functional groups of C=O and C–O, respectively.[36,40,41]

The NMR data analysis, as indicated in Supplementary table 3, revealed that compound CS2 showed proton shifts on carbons C10–C17 as aliphatic alkanes, –CH_2–CH_2 between 1.19 and 1.26 ppm (0.8–1.6 ppm).[45,46] Protons on carbon numbers C18–C23 and C25–C28 indicate the presence of cyclic alkane, CH_2–CH_2–CH with shifts between 1.20 and 1.63 ppm (1.2–1.7 ppm).[6,45,46] Similarly, proton shifts of carbons 5–8, between 5.80 and 7.29 ppm (4.0–7.3 ppm), indicate an alkene, HC=CH.[54,55] A proton shift of 7.66 ppm on carbon 5, =CH, shows that the compound CS2 contains a cyclic alkene.[54] Significantly, on compound CS2, the proton on carbon number 8 indicated an alkyl of ester, –OCH_2 at 4.20 ppm (3.5–4.8 ppm), whilst the proton adjacent to C=O on carbon 10, 2.88 ppm (2.0–3.0 ppm), shows –CH.

Proton on carbon C8 confirms the ester nature of CS2.[54,55] Supplementary table 5 indicates the analysis of ¹³C NMR spectrum, with approximately 19 carbon peaks (δ 10.98, 14.04, 14.11, 22.69, 22.96, 23.79, 24.48, 28.92, 29.37, 29.66, 29.70, 30.41, 31.93, 34.00, 38.74, 66.81, 114.03, 127.58 and 173.57 ppm), as expected given the overlaps in the spectrum, with a strong carbonyl peak at 173.57 ppm, assigned to carbon 9 (Figure 3).

The 2D NMR of the proposed compound, CS2, demonstrates varying coupling dimensions. A typical example is the two protons on carbon 10 close to the carbonyl moiety coupled with the adjacent proton on carbon 9 (Supplementary figure 13) as confirmed by HSQC Supplementary figure 14. Similarly, protons on carbons 12 and 13 can also be confirmed by the HSQC spectrum, which also coupled with each other to give triplets at δ 2.29 and 1.65. The methylene protons
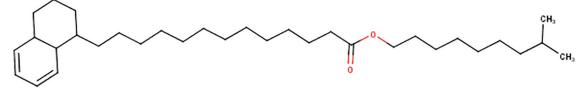

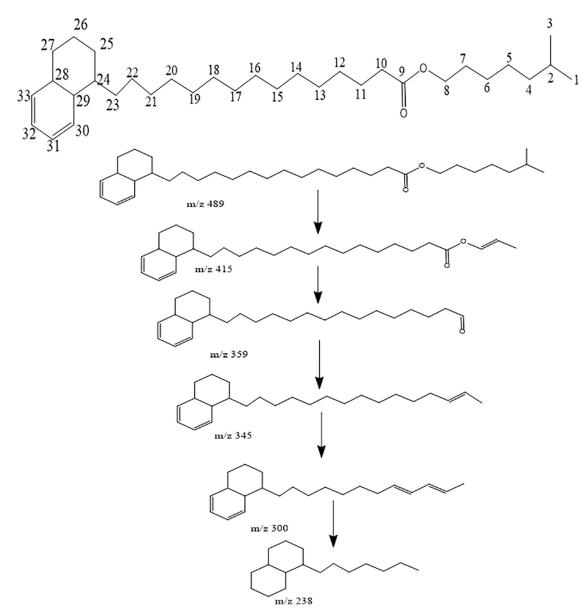**Figure 3:** Proposed structure of CS2–Compound 2.

Figure 4: Fragmentation pattern of CS2 from mass spectroscopy.

between carbon 4 and carbon 8, as well as carbon 14 and 23, shifted up field and overlapped at δ 1.261.

The mass spectrometric analysis of CS2, showed a mass ion peak at *m/z* 489 (M + H), from which a molecular formula of $C_{33}H_{60}O_2$ was assigned (Supplementary figure 4). A retention time of (Rt) of 0.464 min (Table 3) produced a precursor ion at *m/z* 489 [M + H], and fragmentation of this molecule (Figure 4) generated product ions at *m/z* 414, derived from the loss of the isopentyl side chain (–75 Da), and *m/z* 359 due to the loss of propanol (–58 Da), *m/z* 300 also due to loss of the second propanol (–59 Da). Based on these data, in addition to the NMR and FTIR data, molecule CS2 was identified as 6-methylheptyl-15-(1,2,3,4,4a,8a-hexa-hydronaphthalen-1-yl)pentadecanoate. The fragmentation pattern of CS2 was based on the analysis of mass spectroscopy in Supplementary figure 4. The fragmentation pattern is indicated in Figure 4.

Biological activity prediction

A biological activity spectrum for a substance is a list of biological activity types for which the probability to be revealed (Pa) and the probability not to be revealed (Pi) are calculated. Pa and Pi values are independent, and their values vary from 0 to 1. Biological activity spectra were predicted for the two isolated structures of 6-methylheptyl penta-decanoate and 6-methylheptyl-15-(1,2,3,4,4a,8a-hexahydronaphthalen-1-yl)pentadecanoate via PASSonline 2005 version.[56] Generally, in predicting the desired biological activity, Pa > Pi is considered feasible as there is a high chance of the compound revealing that activity. If Pa > 0.7, the compound is likely to reveal its activity in experiments, but in this case, the chance of being the analogue of the known pharmaceutical agent is high. If 0.5 < Pa < 0.7, the compound is likely to reveal this activity in experiments, but this is less, and the compound is not so similar to the known pharmaceutical agent. If Pa < 0.5, the compound is unlikely to reveal this activity in experiments, but if the presence of this activity is confirmed in the experiment, the compound might be a new chemical entity.

The biological activities predicted for each of the compounds herein include antieczematic, antiphobic, and antipruritic for CS1, as shown in Table 4, and antieczematic and antiulcerative for CS2, as shown in Table 4. Findings from the biological activity prediction show that both compounds had diverse activities towards different biological processes. However, the selected compounds were predicted to have a common antiviral property, particularly against rhinovirus.

In this study, special attention was given to certain reported activities of *S. mombin* that actively have antiviral properties.[57,58] Hence, the selection of a suitable biological activity related to the antiviral activity of its isolated compounds, CS1 and CS2, was feasible. Additionally, the desired novelty of a chemical compound is important as well. The predicted Pa values for CS1 (0.655) and CS2 (0.643) both correlated to antiviral activity (rhinovirus), which falls within the 0.5 < Pa < 0.7 threshold correlating to a novel compound that has no known similarity to a known pharmaceutical agent. Subsequently, various antiviral

macromolecules were selected to test the efficiency of CS1 and CS2 via *in silico* molecular docking.

Molecular docking

Molecular docking of selected rhinovirus targets used was human rhinovirus HRV (5FX6), human N-myristoyltransferase-HsNMT1 (5MU6), human N-myristoyltransferases-HsNMT2 (4C2X), and rhinovirus 3C protease (1CQQ). The compounds showed good binding towards the selected targets, as evidenced by obtaining an overall binding affinity in the range of −4.6 to −8.2 kcal/mol across all targets, as shown in Table 5. However, CS1 and CS2 proved to have the best binding affinity when docked to HsNMT1 (5MU6), suggesting they may have potential activity towards the HsMNT1 micromolecule, which is a potential drug target in developing therapeutics against the common cold.

Analysis of molecular dynamic simulation

Molecular dynamic simulations were conducted to assess the conformation dynamics as well as the spatial distribution of atoms in the backbone structure of HsMNT1 upon binding of the compounds. MD simulations were also employed to further validate findings from molecular docking by showing the most stable conformations of the complexed structures across time. Post-MD analysis protocols, including root-mean-square deviation (RMSD), and root-mean-square fluctuation (RMSF), radius of gyration (RoG) and solvent-accessible surface area (SASA), were employed to provide insights on the structural impact of the phytochemical compounds on HsNMT1. An error assessment was also established in analysing all MD trajectories to consider technical and biological variability. Eliminating these systematic errors lowers experimental variability and makes it possible to determine the underlying dynamics of protein motion in cellular signalling with greater accuracy.

Structural stability of HsNMT1

A 150-ns MD simulation trajectory was established to analyse the conformational dynamics of the c-α atoms in the backbone structure of HsNMT1 in all the simulated systems. The root means square deviation gives an estimation of the protein convergence and stability of the simulated system. Furthermore, the RMSD value estimates the average variation in atomic displacement over a given period of time compared to a reference time.[59] The acceptable threshold for an average change in RMSD of a protein-ligand complex is between 1 and 3 Å. If the RMSD average is more significant than this threshold, it implies there is an extensive conformational alteration in the structure of the protein. Findings show that systems converged early during the simulation and maintained steady atomic motions till the 150-ns simulation run, as shown in Figure 5A. The mean RMSD estimated for all the simulated systems were 1.88, 2.15, 1.54 and 1.83 Å for the unbound HsNMT1, 6-methylheptyl pentadecanoate, 6-methylheptyl-15-(1,2,3,4,4a,8a-hexahydronaphthalen-1-yl)pentadecanoate and IMP-1088 complex systems, respectively. As observed from the findings, all systems attained good stability due to the maintenance of mean RMSD values

Table 4: Predicted biological activity via PASSonline

Biological activity					
CS1			CS2		
Pa	Pi	Activity	Pa	Pi	Activity
0.962	0.002	Anti eye irritant	0.868	0.012	Antiphobic
0.944	0.003	Antiphobic	0.757	0.005	Cholesterol antagonist
0.820	0.015	Antieczematic	0.723	0.030	Antieczematic
0.713	0.007	Antipruritic	0.730	0.005	Antiulcerative
0.655	0.004	**Antiviral (rhinovirus)**	0.643	0.013	**Antiviral (rhinovirus)**

Key: Pa, probability to be revealed; Pi, probability not revealed

Table 5: Molecular docking scores

Compound	Binding energy (kcal/mol)			
	HRV (5fx6)	HsNMT1 (5mu6)	HsNMT2 (4c2x)	HRV 3C (1CQQ)
CS1	−4.6	**−7.6**	−7.3	6.5
CS2	−4.2	**−8.2**	−7.9	7.0
Rupintrivir (reference)	−7.7	X	X	X
IMP-1088 (reference)	X	−11	−9.8	X
AG7088 (reference)	X	X	X	6.5

within the acceptable range of 1.5−2.5 Å during the simulation. Also, good stability highlights the reliability of the simulated systems for further conformational analysis.

Structural flexibility of HsNMT1

The root means square fluctuations were assessed to determine the relative flexibility of the c-α atoms in the backbone structure of HsNMT1 upon binding of the inhibitors. As such, the RMSF values of the unbound HsNMT1, CS1, CS2 and IMP-1088 complexed with HsNMT1 were estimated to observe the change in protein structural flexibility during the simulation run. As shown in Figure 5B, all the selected compounds, including the reference IMP-1088 compound, show a peak area of the protein at Glu130, Leu175, Lys240, Ser315 and Thr395 residual positions that fluctuate the most during the simulation. It was observed that the amino acid residues where the reference IMP-1088 bound have similar structural behaviour as that of the phytochemically bound systems of HsMNT1. The mean RMSF values estimated were 0.98 $\pm$ 0.03, 1.01 $\pm$ 0.04, 0.87 $\pm$ 0.02 and 0.95 $\pm$ 0.03 Å for unbound HsNMT1, CS1, CS2 and IMP-1088, respectively, showing that the values are very close to each other. However, in comparing the relative flexibilities of the simulated systems, the complexed HsNMT1 systems show lower fluctuations in contrast to the native unbound system of HsNMT1, indicating that the bound inhibitors enact rigidity on the protein structure.

Radius of gyration

The spatial arrangement of atoms in a protein-ligand complex system around its axis is known as the radius of gyration (RoG).[56,60] Estimating RoG is one of the most crucial indicators for predicting a macromolecule's structural activity, and it provides insights into variations in the compactness of the protein complex. Therefore, the stability of the unbound HsNMT1, CS1, CS2 and IMP-1088 complexes was estimated by measuring RoG over the 150-ns simulation as shown in Figure 5C. The respective RoG averages computed were 21.85,

21.75, 21.77 and 21.78 Å for the Apo (HsNMT1), CS1, CS2 and IMP-1088 systems. The similarity in mean values of the native unbound state (apo) of HsNMT1 and the bound complexes indicates that the selected compounds do not induce major conformational changes to the active site upon binding.

Solvent-accessible surface area

Solvent-accessible surface area (SASA) impacts the structure and activity of biological macromolecules. SASA analysis provides important insights into residual exposure to surrounding solvent molecules during the simulation. Furthermore, due to the location of active site residues at the surface of the protein, greater insight into residue accessibility to solvent would be important in understanding the solvent-like behaviour (hydrophilic or hydrophobic) of a molecule as well as the protein–ligand complex.[61,62] SASA analysis can also be used to describe protein folding and unfolding.[61] As such, the SASA for the simulated systems was computed, as shown in Figure 5D. The averages estimated for the simulated systems were 18570.40, 17877.74, 17707.02 and 18000.32 Å^2 for the Apo (iron-free), CS1, CS2 and Imp-1088, respectively. The SASA values of the complexed systems were slightly lower than those of the unbound HsNMT1 system, indicating a lower surface area exposed to solvent. The binding of the inhibitors induces rigidity in the amino acids in the structure of HsNMT1 upon binding. Findings further highlight the similarity in the structural impact of the compounds and the reference inhibitor of HsNMT1.

Binding free energy

The mechanics/generalised-born surface area (MM/GBSA) method was employed to estimate the binding free energetics of the complexed systems of CS1 and CS2, including the reference IMP-1088 compound. It is well recognised that the MM/GBSA method for predicting binding energy is more accurate than most molecular docking scoring functions and computationally less complex than alchemical free energy techniques.[63-66]

Figure 5: Comparative C-α RMSD, RMSF, RoG and SASA plots showing conformational alterations upon binding of the compounds and reference compound to HsNMT1 over the 150-ns MD simulation time. (A) The RMSD plots, which indicate the compounds induced relative stability on the HsNMT1 enzyme upon binding. (B) The RMSF plots indicating peak regions of residual fluctuations. (C) Relative compactness of all simulated systems of complex structures and the unbound (Apo) system. (D) The surface area exposed to solvent between the simulated systems.

The computed binding free energies for the complexed systems of HsNMT1 were estimated to be −35.20 kcal/mol for CS1, −44.55 kcal/mol for CS2 and −47.06 kcal/mol for IMP-1088. Findings show that CS2 had the strongest binding free energy among the two compounds; however, both compounds demonstrated overall stronger energies than the reference compound used in the study. The results indicate that these compounds can be considered potential inhibitors of HsNMT1. Table 6 indicates the energy terms that contribute to the binding free energy, the most favourable components being the ΔE_{ele}, ΔE_{vdw} and ΔG_{gas}, whilst ΔG_{sol} is unfavourable. The MM/GBSA method is a well-known technique that demonstrates computational effectiveness using implicit solvent and also offers a transparent environment for determining the physical causes of observed effects in protein-ligand interactions.[28,66] Taken together, the energies presented by these compounds suggest the spontaneity, permeation and a measure of the reaction kinetics that characterise their complexing with the target protein.

Binding interactions

The types of interactions a molecule has in a target protein's binding pocket emphasise how therapeutically effective it is for the protein.[67] The binding interactions of CS1, CS2 and the reference IMP-1088 compound bound to HsNMT1 were assessed. The CS1 and CS2 as potential inhibitors were observed to engage in a variety of interactions involving conventional and carbon–hydrogen bonds, van der Waals and pi-alkyl, alkyl interaction as depicted in Figure 5. The variation in interaction types between the potential inhibitors and the binding site residues was attributed to the different molecular features. Assessing the interaction profile of the reference (IMP-1088) compounds showed similar interaction types, as observed in Figure 6. The interactions observed herein include conventional and carbon-hydrogen bonds, van der Waals and pi-alkyl, alkyl interaction, pi–pi stacked, and pi–pi T-shaped. Findings revealed similar interactions with binding site residue between the compounds and the reference compound, suggesting CS1

Table 6: Binding free energy estimations via MM/GBSA

Complexes	ΔE_{vdw}	ΔE_{ele}	ΔG_{gas}	ΔG_{sol}	ΔG_{bind}
HsNMT1-IMP-1088	−44.97 ± 0.33	−47.24 ± 0.39	−82.21 ± 0.27	54.03 ± 0.36	−35.20 ± 0.15
HsNMT1-CS1	53.60 ± 0.23	−10.67 ± 0.18	−64.27 ± 0.30	19.72 ± 0.13	−44.55 ± 0.24
HsNMT1-CS2	−60.19 ± 0.32	−5.28 ± 0.29	−65.45 ± 0.43	18.41 ± 0.24	−47.06 ± 0.28

ΔE_{ele} = electrostatic energy; ΔE_{vdw} = van der Waals energy; ΔG_{bind} = total binding free energy; ΔG_{sol} = solvation-free energy; ΔG = gas-phase free energy
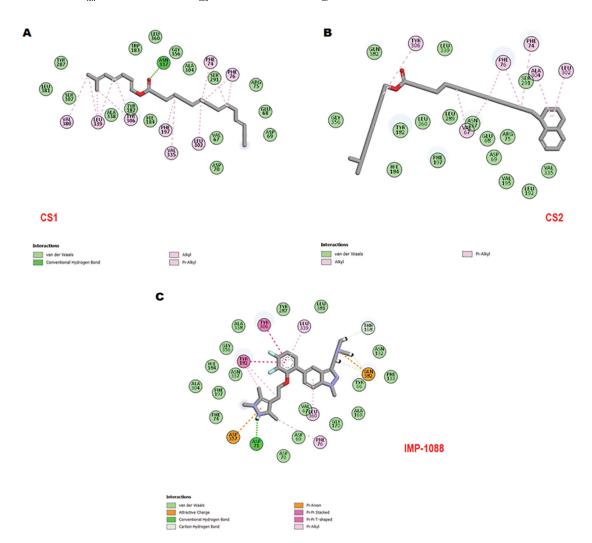

Figure 6: 2D molecular interactions of inhibitors (A) CS1, (B) CS2 and (C) IMP-1088 within the binding site of HsNMT1 showing similar interactions with the binding site residues, suggesting the compounds have the potential to elicit similar therapeutic effects as reference IMP-1088.

and CS2 compounds may have the potential to elicit similar therapeutic effects against HsNMT1.

The outcome of this investigation highlighted several possible biological activities. However, the selection of suitable biological activity was considered based on a higher Pa value than a Pi value. Special attention was given to the reported biological activity associated with the *S. mombin* leaf extracts known to have antiviral activity. Thus, the suitable biological activity predicted for the two isolated novel esters was antiviral activity, particularly towards rhinovirus. Amongst the selected targets, CS1 and CS2 showed a higher binding potential for HsMNT1, an essential enzyme in treating the common cold. The MD simulation employed to test the effect of the compounds against HsNMT1 enzymes revealed that the compounds exhibited good stability, flexibility, structural rigidity, and reduced surface area exposed to solvents. These structural effects of the compounds towards HsNMT1 were similar to the structural effects of the reference inhibitor, suggesting the potential inhibitory effects of the compounds towards HsNMT1.

In silico molecular recognition protocols were employed to assess the pharmacological effects of the compounds CS1 and CS2 on the *S. mombin* leaf. The predicted biological activity for the two isolated novel esters was anti-rhinovirus activity.

Molecular docking analysis indicated that CS1 and CS2 showed a higher binding potential towards HsMNT1. The MM/GBSA method revealed stronger binding free energy in CS1 and CS2 than the reference compound. Assessment of binding interactions also shows similarity in interactions CS1, CS2 and the reference IMP-1088 inhibitor, indicating the potential to elicit similar therapeutic effects against HsNMT.

Conclusion

The current study of the phytochemical analysis of DCM leaf extracts of *S. mombin* led to the identification of two esters that had previously not been reported in the plant. These compounds, 6-methylheptyl penta-decanoate and 6-methylheptyl-15-(1,2,3,4,4a,8a-hexahydronaphthalen-1-yl)pentadecanoate, possess anti-rhino virus (HsNMT1) properties as indicated through an *in silico* molecular targeting prediction.

Further in vitro validation is required to optimise a potential drug candidate.

Funding

No funding was obtained.

Data availability

The data supporting the results of this study are included in the article and as supplementary material.

Declaration of AI use

AI was not used in the conceptualisation or preparation of the manuscript.

Authors' contributions

A.B.: Conceptualisation, data collection, data analysis, writing – the initial draft. R.K.: Student supervision. M.N.: Student supervision. All authors read and approved the final manuscript.

Competing interests

The authors declare that they have no known competing financial interests or personal relationships that could have influenced the work reported here.

References

1. Sasidharan S, Chen Y, Saravanan D, Sundram K, Latha LY. Extraction, isolation and characterization of bioactive compounds from plants' extracts. Afr J Tradit Complement Altern Med. 2011; 8(1), Art. #60483. https://doi.org/10.4314/ajtcam.v8i1.60483

2. Anand U, Jacobo-Herrera N, Altemimi A, Lakhssassi N. A comprehensive review on medicinal plants as antimicrobial therapeutics: Potential avenues of biocompatible drug discovery. Metabolites. 2019; 9(11), Art. # 258. https://doi.org/10.3390/metabo9110258

3. Mukherjee PK, Rai S, Kumar V, Mukherjee K, Hylands P, Hider R. Plants of Indian origin in drug discovery. Expert Opin Drug Discov. 2007; 2(5): 633–657. https://doi.org/10.1517/17460441.2.5.633

4. Balunas MJ, Kinghorn AD. Drug discovery from medicinal plants. Life Sci. 2005; 78(5): 431–441. https://doi.org/10.1016/j.lfs.2005.09.012

5. Mustafa G, Arif R, Atta A, Sharif S, Jamil A. Bioactive compounds from medicinal plants and their importance in drug discovery in Pakistan. Matrix Sci Pharma. 2017; 1(1): 17–26. https://doi.org/10.26480/msp.01.2017.17.26

6. Osuntokun OT. Synergistic efficacy of *Aframomum melegueta* [Roscoe] K. Schum and *Spondias mombin* (Linn), A predictive treatment of SARS-CoV-2 (COVID-19) Infection. J Biosci Bioeng. 2020; 1(2): 1–8.

7. Fred-Jaiyesimi A, Kio A, Richard W. α-Amylase inhibitory effect of 3β-olean-12-en-3-yl (9Z)-hexadec-9-enoate isolated from *Spondias mombin* leaf. Food Chem. 2009; 116(1): 285–288. https://doi.org/10.1016/j.foodchem.2009.02.047

8. Corthout J, Pieters L, Claeys M, Berghe DV, Vlietinck A. Antiviral caffeoyl esters from *Spondias mombin*. Phytochemistry. 1992; 31(6): 1979–1981. https://doi.org/10.1016/0031-9422(92)80344-E

9. Ojo OA, Afon AA, Ojo AB, Ajiboye BO, Oyinloye BE, Kappo AP. Inhibitory effects of solvent-partitioned fractions of two Nigerian herbs (*Spondias mombin* Linn. and *Mangifera indica* L.) on α-amylase and α-glucosidase. Antioxididants. 2018; 7(6), Art. # 73. https://doi.org/10.3390/antiox7060073

10. dos Santos Sampaio TI, de Melo NC, de Freitas Paiva BT, da Silva Aleluia GA, da Silva Neto FLP, da Silva HR , et al. Leaves of *Spondias mombin* L. a traditional anxiolytic and antidepressant: Pharmacological evaluation on zebrafish (*Danio rerio*). J Ethnopharmacol. 2018; 224: 563–578. https://doi.org/10.1016/j.jep.2018.05.037

11. Cock IE, Van Vuuren SF. The traditional use of southern African medicinal plants in the treatment of viral respiratory diseases: A review of the ethnobotany and scientific evaluations. J Ethnopharmacol. 2020; 262, Art. # 113194. https://doi.org/10.1016/j.jep.2020.113194

12. Drysdale SB, Mejias A, Ramilo O. Rhinovirus-not just the common cold. J Infect. 2017; 74:S41–S46. https://doi.org/10.1016/S0163-4453(17)30190-1

13. Revathi N, Dhanaraj T. Evaluation of bioactive phytochemicals in leaves extract of *Dodonaea angustifolia* using gas chromatography and mass spectroscopic technique. J Pharmacogn Phytochem. 2019; 8(3): 4406–4409.

14. Talukdar AD, Choudhury MD, Chakraborty M, Dutta B. Phytochemical screening and TLC profiling of plant extracts of *Cyathea gigantea* (Wall. Ex. Hook.) Haltt. and *Cyathea brunoniana*. Wall. ex. Hook (Cl. & Bak.). Assam Univ J Sci Technol. 2010; 5(1): 70–74.

15. Uli H, Noor A, Mandey FW, Sapar A. Isolation, identification and bioactivity test of non polar compounds on N-hexane extract of *Haliclona (Reniera) fascigera* from Samalona Island-Spermonde Archipelago. Marina Chimica Acta. 2016; 17(2).

16. Varnek A, Tropsha A, editors. Chemoinformatics approaches to virtual screening. Cambridge: Royal Society of Chemistry; 2008 . https://doi.org/10.1039/9781847558879

17. Lagunin A, Stepanchikova A, Filimonov D, Poroikov V. Internet server for on-line prediction of the biological activity spectrum for a substance. Bioinformatics. 2000; 16(8): 747–748. https://doi.org/10.1093/bioinformatics/16.8.747

18. Jairajpuri DS, Hussain A, Nasreen K, Mohammad T, Anjum F, Rehman MT , et al. Identification of natural compounds as potent inhibitors of SARS-CoV-2 main protease using combined docking and molecular dynamics simulations. Saudi J Biol Sci. 2021; 28(4): 2423–2431. https://doi.org/10.1016/j.sjbs.2021.01.040

19. Cheng Z, Wu T. TLC bioautography: High throughput technique for screening of bioactive natural products. Comb Chem High T Scr. 2013; 16(7): 531–549. https://doi.org/10.2174/1386207311316070004

20. Djide MN. Sartini. Analisis mikrobiologi farmasi [Pharmaceutical microbiology analysis]. Makassar: Laboratory of Pharmaceutical Microbiology and Pharmaceutical Biotechnology, Faculty of Mathematics and Natural Sciences, Hasanudin University; 2008. Indonesian.

21. Shaikh JR, Patil M. Qualitative tests for preliminary phytochemical screening: An overview. Int J Chem Stud. 2020; 8(2): 603–608. https://doi.org/10.22271/chemi.2020.v8.i2i.8834

22. Pandith JI. Phytochemical screening of certain plant species of Agra city. J Drug Deliv Ther. 2012; 2(4), Art. #212. https://doi.org/10.22270/jddt.v2i4.212

23. Hofmann MH, Gmachl M, Ramharter J, Savarese F, Gerlach D, Marszalek JR, et al. Bi-3406, a potent and selective SOS1-KRAS interaction inhibitor, is effective in KRAS-driven cancers through combined MEK Inhibitionpan-KRAS SOS1 protein-protein interaction inhibitor Bi-3406. Cancer Discov. 2021; 11(1): 142– 157. https://doi.org/10.1158/2159-8290.CD-20-0142

24. Berman HM, Westbrook J, Feng Z, Gilliland G, Bhat TN, Weissig H, et al. The protein data bank. Nucleic Acids Res. 2000; 28(1): 235– 242. https://doi.org/10.1093/nar/28.1.235

25. Eric FP, Thomas DG, Conrad CH, Gregory SC, Daniel MG, Elaine CM, et al. UCSF Chimera? A visualization system for exploratory research and analysis. J Comput Chem. 2004; 25(13): 1605– 1612. https://doi.org/10.1002/jcc.20084

26. Webb B, Sali A. Protein structure modeling with *MODELLER*. In: Kihara D, editors. Protein structure prediction: Methods in molecular biology. Volume 1137. New York: Humana Press; 2014. p. 1–15. https://doi.org/10.1007/978-1-4939-0366-5_1

27. Massova I, Kollman PA. Combined molecular mechanical and continuum solvent approach (MM-PBSA/GBSA) to predict ligand binding. Perspect Drug Discovery Des. 2000; 18(1): 113– 135. https://doi.org/10.1023/A:1008763014207

28. Genheden S, Kuhn O, Mikulskis P, Hoffmann D, Ryde U. The normal-mode entropy in the MM/GBSA method: Effect of system truncation, buffer region, and dielectric constant. J Chem Inf Model. 2012; 52(8): 2079– 2088. https://doi.org/10.1021/ci3001919

29. Sitkoff D, Sharp KA, Honig B. Accurate calculation of hydration free energies using macroscopic solvent models. J Phys Chem. 1994; 98(7): 1978– 1988. https://doi.org/10.1021/j100058a043

30. Ugadu AF, Ominyi M, Ogbanshi M, Eze U. Phytochemical analysis of Spondias mombin. Int J Innov Res Dev. 2014; 3(9): 101– 107.

31. Sameh S, Al-Sayed E, Labib RM, Singab AN. Genus *Spondias*: A phytochemical and pharmacological review. Evid Based Complement Alternat Med. 2018; 2018, Art. #5382904. https://doi.org/10.1155/2018/5382904

32. Salifu EY, Issahaku AR, Agoni C, Ibrahim MA, Manimbulu N, Soliman ME. Prioritizing the catalytic gatekeepers through Pan-inhibitory mechanism of entrectinib against ALK, ROS1 and TrkA tyrosine kinases. Cell Biochem Biophys. 2022; 80(1): 11– 21. https://doi.org/10.1007/s12013-021-01052-2

33. Salifu EY, Agoni C, Soliman ME. Highlighting the mechanistic role of Olutasidenib (FT-2102) in the selective inhibition of mutated isocitrate dehydrogenase 1 (mIDH1) in cancer therapy. Inform Med Unlocked. 2022; 28, Art. # 100829. https://doi.org/10.1016/j.imu.2021.100829

34. Genheden S, Ryde U. The MM/PBSA and MM/GBSA methods to estimate ligand-binding affinities. Expert Opin Drug Discov. 2015; 10(5): 449– 461. https://doi.org/10.1517/17460441.2015.1032936

35. Durrant JD, McCammon JA. Molecular dynamics simulations and drug discovery. BMC Biol. 2011; 9(1): 1– 9. https://doi.org/10.1186/1741-7007-9-71

36. Quach HT, Steeper RL, Griffin GW. An improved method for the extraction and thin-layer chromatography of chlorophyll a and b from spinach. J Chem Educ. 2004; 81(3), Art. # 385. https://doi.org/10.1021/ed081p385

37. Sathya S. Separation of algal pigments by thin layer chromatography (TLC) and high performance liquid chromatography (HPLC). World J Pharm Res. 2017; 6: 1275– 1284.

38. Sherma J, Fried B. Handbook of thin-layer chromatography. 3rd ed. Boca Raton, FL: CRC Press; 2003. https://doi.org/10.1201/9780203912430

39. Hamberg M, Samuelsson B. Prostaglandin endoperoxides. Novel transformations of arachidonic acid in human platelets. Proc Natl Acad Sci USA. 1974; 71(9): 3400– 3404. https://doi.org/10.1073/pnas.71.9.3400

40. Wang Y, Han Y, Hu W, Fu D, Wang G. Analytical strategies for chemical characterization of bio-oil. J Sep Sci. 2020; 43(1): 360– 371. https://doi.org/10.1002/jssc.201901014

41. Baruah N, Dey SS, Nayak SK. Evaluation of dissolved gas analysis and long-term performance of non-edible natural ester. IEEE Trans Dielectr Electr Insul. 2020; 27(5): 1561– 1569. https://doi.org/10.1109/TDEI.2020.008768

42. Pratheeba T, Ragavendran C, Natarajan D. Larvicidal, pupicidal and adulticidal potential of Ocimum gratissimum plant leaf extracts against filariasis inducing vector. Int J Mosq Res. 2015; 2(2): 1– 8.

43. Udo GJ, Etesin UM, Awaka-Ama JJ, Nyong AE, Uwanta EJ. GCMS and FTIR spectroscopy characterization of *Luffa cylindrica* seed oil and biodiesel produced from the oil. Comm Phys Sci. 2010; 5(1–3).

44. Socrates G. Infrared and Raman characteristic group frequencies: Tables and charts. Hoboken, NJ: John Wiley & Sons; 2004.

45. Silverstein R, Bassler GC, Morrill TC. Sptrometric identification of organic compounds. New York: Wiley; 1981.

46. Jain P, Soni A, Jain P, Bhawsar J. Phytochemical analysis of *Mentha spicata* plant extract using UV-VIS, FTIR and GC/MS technique. J Chem Pharm Res. 2016; 8(2): 1– 6.

47. Karthikaiselvi R, Subhashini S. Study of adsorption properties and inhibition of mild steel corrosion in hydrochloric acid media by water soluble composite poly (vinyl alcohol-o-methoxy aniline). J Assoc Arab Univ Basic Appl Sci. 2014; 16: 74– 82. https://doi.org/10.1016/j.jaubas.2013.06.002

48. Pramila D, Xavier R, Marimuthu K, Kathiresan S, Khoo M, Senthilkumar M, et al. Phytochemical analysis and antimicrobial potential of methanolic leaf extract of peppermint (*Mentha piperita*: Lamiaceae). J Med Plant Res. 2012; 6(2): 331– 335. https://doi.org/10.5897/JMPR11.1232

49. Rakhmatullin IZ, Efimov SV, Klochkov AV, Gnezdilov OI, Varfolomeev MA, Klochkov VV. NMR chemical shifts of carbon atoms and characteristic shift ranges in the oil sample. Pet Res. 2022; 7(2): 269– 274. https://doi.org/10.1016/j.ptlrs.2021.10.001

50. Osuntokun OT, Idowu T, Gamberini MC. Bio-guided isolation, purification and chemical characterization of epigallocatechin; epicatechin, stigmasterol, phytosterol from ethyl acetate stem bark fraction of *Spondias mombin* (Linn.). Biochem Pharmacol. 2018; 7: 1. https://doi.org/10.4172/2167-0501.1000240

51. López-Camacho PY, Martínez-Espinosa JC, Basurto-Islas G, Torres-Zarraga A, Márquez-Villa JM, Macías-Alonso M, et al. *Spondias mombin* seed oil compounds identification by raman spectroscopy and NMR. Appl Sci. 2021; 11(6), Art. # 2886. https://doi.org/10.3390/app11062886

52. Buckingham A. Chemical shifts in the nuclear magnetic resonance spectra of molecules containing polar groups. Can J Chem. 1960; 38(2): 300– 307. https://doi.org/10.1139/v60-040

53. Cao X, Lattao C, Pignatello JJ, Mao J, Schmidt-Rohr K. Sorption selectivity in natural organic matter probed with fully deuterium-exchanged and carbonyl-13C-labeled benzophenone and 1H-13C NMR spectroscopy. Environ Sci Technol. 2014; 48(15): 8645– 8652. https://doi.org/10.1021/es501129f

54. Wu Q, Yu S, Hao N, Wells T Jr, Meng X, Li M, et al. Characterization of products from hydrothermal carbonization of pine. Bioresour Technol. 2017; 244: 78– 83. https://doi.org/10.1016/j.biortech.2017.07.138

55. Neiens SD, Geißlitz SM, Steinhaus M. Aroma-active compounds in *Spondias mombin* L. fruit pulp. Eur Food Res Technol. 2017; 243(6): 1073– 1081. https://doi.org/10.1007/s00217-016-2825-7

56. Zheng C, Zhu M, Zhang D. Characterisation of asphaltenes extracted from an Indonesian oil sand using NMR, DEPT and MALDI-TOF. Energy Procedia. 2015; 75: 847– 852. https://doi.org/10.1016/j.egypro.2015.07.176

57. David AA, Oladele AA, Philip AO, Zabdiel AA, Olufunso AB, Tolulope OO, et al. Tropical Journal of natural product research. 2022;6(2):281–286.

58. Elufioye TO, Obuotor EM, Agbedahunsi JM, Adesanya SA. Anticholinesterase constituents from the leaves of *Spondias mombin* L.(Anacardiaceae). Biologics: Targets & Therapy. 2017; 11, Art. # 107. https://doi.org/10.2147/BTT.S136011

59. Echeme JO, Ahuchogu AA, Uchegbu RI. *Spondias mombin* Linn. Am J Chem Appl. 2014; 1(3): 28– 31.

60. Huynh T, Smith JC, Sanson A. Protein unfolding transitions in an intrinsically unstable annexin domain: Molecular dynamics simulation and comparison with nuclear magnetic resonance data. Biophys J. 2002; 83(2): 681– 698. https://doi.org/10.1016/S0006-3495(02)75200-4

61. Osuntokun O, Ige O, Idowu T, Gamberini M. Bio-activity and spectral analysis of gas chromatography/mass spectroscopy (GCMS) profile of crude *Spondias mombin* extracts. SciFed J Anal Biochem. 2018; 1(2): 1– 12.

62. Fred-Jaiyesimi AA, Wilkins RM, Abo KA. Glucose lowering activities of mombintane I and mombintane II isolated from the leaves of *Spondias mombin* L. Int J Biol Chem Sci. 2017; 11(3): 1315– 1319. https://doi.org/10.4314/ijbcs.v11i3.31

63. Kufareva I, Abagyan R. Methods of protein structure comparison. In: Orry A, Abagyan R, editors. Homology modeling. Methods in molecular biology. Volume 857. Totowa, NJ: Humana Press ; 2011. p. 231– 257. https://doi.org /10.1007/978-1-61779-588-6_10

64. Mlu L, Bogatyreva N, Galzitskaia O. Radius of gyration is indicator of compactness of protein structure. Mol Biol. 2008; 42(4): 701– 706. https:// doi.org/10.1134/S0026893308040195

65. Durham E, Dorr B, Woetzel N, Staritzbichler R, Meiler J. Solvent accessible surface area approximations for rapid and accurate protein structure prediction. J Mol Model. 2009; 15(9): 1093– 1108. https://doi.org/10.100 7/s00894-009-0454-9

66. Tiwari A, Mukherjee B, Dixit M. MicroRNA key to angiogenesis regulation: miRNA biology and therapy. Curr Cancer Drug Targets. 2018; 18(3): 266– 277. https://doi.org/10.2174/1568009617666170630142725

67. Xue J, Huang X, Zhu Y. Using molecular dynamics simulations to evaluate active designs of cephradine hydrolase by molecular mechanics/Poisson-Boltzmann surface area and molecular mechanics/generalized Born surface area methods. RSC Adv. 2019; 9(24): 13868– 13877. https://doi.org/10.10 39/C9RA02406A